

Article

# Enhanced Low Temperature NO Reduction Performance via MnO<sub>x</sub>-Fe<sub>2</sub>O<sub>3</sub>/Vermiculite Monolithic Honeycomb Catalysts

Ke Zhang <sup>1</sup>, Feng Yu <sup>1,\*</sup>, Mingyuan Zhu <sup>1</sup>, Jianming Dan <sup>1,2,3</sup>, Xugen Wang <sup>1</sup>, Jinli Zhang <sup>1</sup> and Bin Dai <sup>1,\*</sup>

<sup>1</sup> Key Laboratory for Green Processing of Chemical Engineering of Xinjiang Bingtuan, School of Chemistry and Chemical Engineering, Shihezi University, Shihezi 832003, China; kezhang1014@163.com (K.Z.); zhumin yuan@shzu.edu.cn (M.Z.); djm\_tea@shzu.edu.cn (J.D.); wxgen@shzu.edu.cn (X.W.); zhangjinli@tju.edu.cn (J.Z.)

<sup>2</sup> Key Laboratory of Materials-Oriented Chemical Engineering of Xinjiang Uygur Autonomous Region, Shihezi 832003, China

<sup>3</sup> Engineering Research Center of Materials-Oriented Chemical Engineering of Xinjiang Production and Construction Corps, Shihezi 832003, China

\* Correspondence: yufeng05@mail.ipc.ac.cn (F.Y.); db\_tea@shzu.edu.cn (B.D.); Tel.: +86-993-205-7272 (F.Y. & B.D.); Fax: +86-993-205-7270 (F.Y. & B.D.)

Received: 31 January 2018; Accepted: 27 February 2018; Published: 28 February 2018

**Abstract:** Selective catalytic reduction of NO<sub>x</sub> by ammonia (NH<sub>3</sub>-SCR) was the most efficient and economic technology for De-NO<sub>x</sub> applications. Therefore, a series of MnO<sub>x</sub>/vermiculite (VMT) and MnO<sub>x</sub>-Fe<sub>2</sub>O<sub>3</sub>/VMT catalysts were prepared by an impregnation method for the selective catalytic reduction (SCR) of nitrogen oxides (NO<sub>x</sub>). The MnO<sub>x</sub>-Fe<sub>2</sub>O<sub>3</sub>/VMT catalysts provided an excellent NO conversion of 96.5% at 200 °C with a gas hourly space velocity (GHSV) of 30,000 h<sup>-1</sup> and an NO concentration of 500 ppm. X-ray photoelectron spectroscopy results indicated that the Mn and Fe oxides of the MnO<sub>x</sub>-Fe<sub>2</sub>O<sub>3</sub>/VMT catalyst were mainly composed of MnO<sub>2</sub> and Fe<sub>2</sub>O<sub>3</sub>. However, the MnO<sub>2</sub> and Fe<sub>2</sub>O<sub>3</sub> components were well dispersed because no discernible MnO<sub>2</sub> and Fe<sub>2</sub>O<sub>3</sub> phases were observed in X-ray powder diffraction spectra. Corresponding MnO<sub>x</sub>-Fe<sub>2</sub>O<sub>3</sub>/VMT monolithic honeycomb catalysts (MHCs) were prepared by an extrusion method, and the MHCs achieved excellent SCR activity at low temperature, with an NO conversion greater than 98.6% at 150 °C and a GHSV of 4000 h<sup>-1</sup>. In particular, the MnO<sub>x</sub>-Fe<sub>2</sub>O<sub>3</sub>/VMT MHCs provided a good SCR activity at room temperature (20 °C), with an NO conversion of 62.2% (GHSV = 1000 h<sup>-1</sup>). In addition, the NO reduction performance of the MnO<sub>x</sub>-Fe<sub>2</sub>O<sub>3</sub>/VMT MHCs also demonstrated an excellent SO<sub>2</sub> resistance.

**Keywords:** MnO<sub>x</sub>-Fe<sub>2</sub>O<sub>3</sub>/vermiculite; monolithic honeycomb catalyst; room-temperature catalysis; selective catalytic reduction; NO removal efficiency

## 1. Introduction

Nitrogen oxides (NO<sub>x</sub>) in stationary stack source emissions are strong contributing factors of acid rain, photochemical smog, and ozone depletion and are, therefore, detrimental to the natural environment and human health [1–3]. Therefore, the selective catalytic reduction (SCR) of NO<sub>x</sub> by ammonia (NH<sub>3</sub>-SCR) was developed to reduce the release of NO<sub>x</sub> (i.e., De-NO<sub>x</sub>), and this has thus far been the most economical and effective technology for De-NO<sub>x</sub> applications [4]. It is well known that the key component affecting the SCR and economic performance of NH<sub>3</sub>-SCR technology is the catalyst employed in the process, which should be low in cost, and provide high SCR activity at low temperatures. As a result, manganese-based catalysts have been widely studied over the past few

decades owing to their low cost and promisingly high SCR activity at low temperature [5]. However, the SCR activity of pure  $\text{MnO}_x$  catalysts is profoundly deteriorated by  $\text{SO}_2$  and  $\text{H}_2\text{O}$ , and emissions with high concentrations of  $\text{SO}_2$  and  $\text{H}_2\text{O}$  can lead to poisoning and the eventual deactivation of pure  $\text{MnO}_x$  catalysts. These drawbacks can be overcome, and the SCR activity of pure  $\text{MnO}_x$  catalysts can even be improved by incorporating transition metal or rare earth elements as catalyst promoters [6,7]. For example, Chen et al. reported that Fe- $\text{MnO}_x$  mixed-oxide catalysts provided a 100%  $\text{NO}_x$  conversion in the temperature range from 140 °C to 220 °C [8].

Since SCR activity occurs on the surfaces of catalysts, the SCR activity of catalysts can be greatly enhanced, particularly under low-temperature conditions, by maximizing their surface area via distribution over high surface area supports. Numerous types of supports have been employed for Mn-based catalysts, such as molecular sieves, carbon materials, and metal oxides. Molecular sieves modified with Mn-based catalyst materials have shown excellent SCR activity because of their regular pore structures, high strength, and high specific surface areas [9]. Numerous Mn-based molecular sieve supported catalysts, such as Mn supported on ZSM-5 zeolite (denoted as Mn/ZSM-5) [10] and  $\text{MnO}_x$ /silicoaluminophosphate zeolite (SAPO-34) [11], have been shown to be highly active for  $\text{NO}_x$  reduction at low temperatures. Carbon materials have also been widely used as catalyst supports because of their well-developed porosity, high specific surface area, chemical stability, strong adsorption ability, and excellent thermal conductivity [12]. For example, Lu et al. synthesized  $\text{MnO}_2$  supported on carbon nanotubes (CNTs), and the catalyst attained an NO conversion of 89.5% at 180 °C [13]. Finally, metal oxide supports provide high catalyst surface areas, high thermal stability, and surface acid-base properties [14,15]. Manganese-based catalysts supported on metal oxides, such as  $\text{MnO}_x/\text{TiO}_2$  [16–18],  $\text{MnO}_x/\text{Al}_2\text{O}_3$  [19],  $\text{MnO}_x/\text{CeO}_2$  [20–22], and  $\text{MnO}_x/\text{Ce-ZrO}_2$  [23], have generated considerable attention, and represent promising catalysts for the SCR of  $\text{NO}_x$  at low temperatures.

In recent years, many researchers have focused on catalysts employing supports composed of natural ore materials, such as montmorillonite, saponite, attapulgite, chabazite, and vermiculite (VMT), due to their great abundance, which makes them easily obtainable and inexpensive materials. A number of catalysts have incorporated these natural ore materials, such as Zr-Mn/attapulgite (ATP) [24], Ce- $\text{MnO}_x$ /ATP [25], porous clay hetero-structures (PCH) modified with  $\text{NH}_3$ -Cu [26], Cu-chabazite (CHA) [27–29] and crystalline  $\text{MnO}_2$  (c- $\text{MnO}_2$ )/ $\text{TiO}_2$ -palygorskite (PAL) [30]. Among the available natural ore materials, the unique layered structure of VMT makes it an excellent candidate as a support for the SCR of NO. In addition, VMT includes metal oxides that can actively assist in catalytic reactions, and its great abundance in Xinjiang, China makes this material of particular interest to Chinese researchers. Chmielarz et al. investigated PCHs based on montmorillonite, saponite, and VMT modified with Fe or Cu as catalysts [31]. Among these catalysts, PCHs involving VMT achieved the best SCR activity at 400 °C. Samojeden et al. developed VMT supports prepared by modifications with nitric acid, and the resulting catalysts formed by impregnation with Cu provided an NO conversion of 94.3% at 350 °C [32]. Moreover, VMT has been widely investigated for use in heterogeneous catalysts, such as in the photocatalyst  $\text{TiO}_2$ /VMT [33], NiO/VMT for carbon monoxide methanation [34,35], and a novel  $\text{HgCl}_2$ /EML-VMT-C catalyst employing expanded multilayered (EML) VMT mixed with carbon on the surface (EML-VMT-C) for the hydrochlorination of acetylene [36]. However, the application of catalysts employing VMT supports for the SCR of  $\text{NO}_x$  at low temperatures remains challenging.

In light of the substantial cost benefits associated with the use of natural ore materials as catalyst supports, the present study employs VMT as supports in the fabrication of  $\text{MnO}_x$ - $\text{Fe}_2\text{O}_3$ /VMT catalysts by the impregnation method for the SCR of NO by  $\text{NH}_3$ . The as-prepared  $\text{MnO}_x$ - $\text{Fe}_2\text{O}_3$ /VMT catalysts provide an excellent NO conversion of 96.5% at 200 °C with a gas hourly space velocity (GHSV) of 30,000  $\text{h}^{-1}$ . To improve the low temperature performance, corresponding  $\text{MnO}_x$ - $\text{Fe}_2\text{O}_3$ /VMT monolithic honeycomb catalysts (MHCs) were prepared by an extrusion method, and the MHCs achieve an NO conversion greater than 98.6% at 150 °C and GHSV = 4000  $\text{h}^{-1}$ . In particular, the  $\text{MnO}_x$ - $\text{Fe}_2\text{O}_3$ /VMT MHCs provided good SCR activity at room temperature (20 °C), with an NO conversion of 62.2% (GHSV = 1000  $\text{h}^{-1}$ ). Finally, because flue gases still contain small amounts of  $\text{SO}_2$

after desulfurization and water removal, we also investigated the influence of  $\text{SO}_2$  on the catalytic performance of  $\text{MnO}_x\text{-Fe}_2\text{O}_3/\text{VMT}$  MHCs.

## 2. Results and Discussion

The results of catalytic activity testing for the as-prepared  $\text{MnO}_x/\text{VMT}$  and  $\text{MnO}_x\text{-Fe}_2\text{O}_3/\text{VMT}$  catalysts are shown in Figure 1. As shown in Figure 1a, the NO conversion of the  $\text{MnO}_x/\text{VMT}$  and  $\text{MnO}_x\text{-Fe}_2\text{O}_3/\text{VMT}$  catalysts increased obviously with increasing temperature in the low temperature region until attaining a maximum value, after which the NO conversion decreased. The highest NO conversion attained for the  $\text{MnO}_x\text{-Fe}_2\text{O}_3/\text{VMT}$  catalyst was 96.5% at 200 °C, while the highest NO conversion attained for the  $\text{MnO}_x/\text{VMT}$  catalyst was 93.1% at 250 °C. Compared with the  $\text{MnO}_x/\text{VMT}$  catalyst, the catalytic activity of the  $\text{MnO}_x\text{-Fe}_2\text{O}_3/\text{VMT}$  catalyst was between 6% and 16% greater than that of the  $\text{MnO}_x/\text{VMT}$  catalyst in the low temperature range of 20–200 °C, indicating that the addition of Fe obviously increased the low temperature activity of the catalyst. For both catalysts, the declining NO conversion at relatively high temperatures originated from the oxidation of the ammonia.

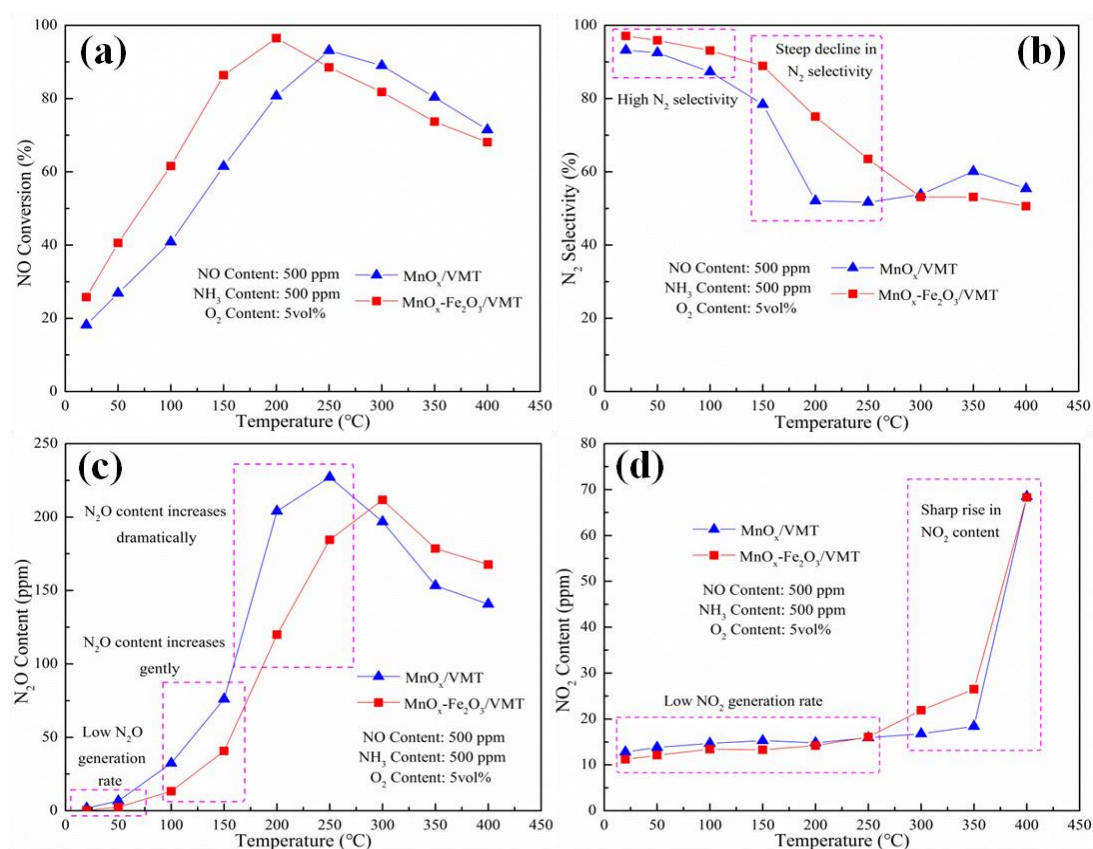


**Figure 1** Catalytic activity of  $\text{MnO}_x/\text{VMT}$  and  $\text{MnO}_x\text{-Fe}_2\text{O}_3/\text{VMT}$  catalyst samples: (a) NO conversion; (b)  $\text{N}_2$  selectivity; (c)  $\text{N}_2\text{O}$  content; and (d)  $\text{NO}_2$  content ( $\text{N}_2$  as balance gas, GHSV = 30,000  $\text{h}^{-1}$ ).

In addition, Figure 1b shows that the  $\text{N}_2$  selectivity of the  $\text{MnO}_x/\text{VMT}$  and  $\text{MnO}_x\text{-Fe}_2\text{O}_3/\text{VMT}$  catalysts gradually declined with increasing temperature in the low temperature region (20–100 °C), and sharply declined in the middle temperature region (150–200 °C). The  $\text{MnO}_x\text{-Fe}_2\text{O}_3/\text{VMT}$  catalyst exhibited excellent  $\text{N}_2$  selectivities of 97.1% and 95.9% at 20 °C and 50 °C, respectively, and its  $\text{N}_2$  selectivity was greater than that of the  $\text{MnO}_x/\text{VMT}$  catalyst at temperatures less than 250 °C. However, we note that the sharp drop in the  $\text{N}_2$  selectivity of the  $\text{MnO}_x\text{-Fe}_2\text{O}_3/\text{VMT}$  catalyst at 150 °C resulted in an  $\text{N}_2$  selectivity that was less than that of the  $\text{MnO}_x/\text{VMT}$  catalyst at temperatures greater than 250 °C. The  $\text{N}_2$  selectivity results are readily correlated with the measured  $\text{N}_2\text{O}$  and  $\text{NO}_2$  contents shown in Figure 1c,d, respectively. Here, we note that the gradual decline in the  $\text{N}_2$  selectivity of both catalysts at low temperature corresponds with a gradually increasing generation of  $\text{N}_2\text{O}$  and  $\text{NO}_2$

over a similar temperature range. In addition, the sharply declining  $N_2$  selectivity of both catalysts in the middle temperature region is mainly because the  $N_2O$  content is increasing rapidly for temperatures greater than  $150\text{ }^\circ\text{C}$ . We also note that the region over which the  $N_2$  selectivity of the  $MnO_x/VMT$  catalyst was greater than that of the  $MnO_x-Fe_2O_3/VMT$  catalyst (i.e., at temperatures greater than  $250\text{ }^\circ\text{C}$ ) corresponds with the fact that both the  $N_2O$  and the  $NO_2$  contents were less for the  $MnO_x/VMT$  catalyst than for the  $MnO_x-Fe_2O_3/VMT$  catalyst at temperatures greater than  $250\text{ }^\circ\text{C}$ . Nevertheless, we note that the  $MnO_x-Fe_2O_3/VMT$  catalyst demonstrated both a better  $NO$  conversion and a better  $N_2$  selectivity than those of the  $MnO_x/VMT$  catalyst in the temperature range of  $20\text{--}200\text{ }^\circ\text{C}$ .

Figure 2a presents X-ray diffractometer (XRD) patterns of the VMT support and as-prepared  $MnO_x/VMT$  and  $MnO_x-Fe_2O_3/VMT$  powdered catalyst samples. We note that VMT presents several strong peaks that exhibit greatly decreased intensities after impregnation. In addition, several diffraction peaks indicative of  $Mn_3O_4$  (PDF#18-0803) are observed for the  $MnO_x/VMT$  catalyst at  $18.1^\circ$ ,  $29.2^\circ$ ,  $32.4^\circ$ ,  $36.2^\circ$ ,  $51.0^\circ$ , and  $58.5^\circ$ , while no other crystal phases of  $MnO_x$  are evident. These results suggest that the existence of diffraction peaks could be due to large crystals of  $MnO_x$ , resulting in weak XRD peaks indicative of  $MnO_x$  and VMT [37]. The  $MnO_x-Fe_2O_3/VMT$  catalyst sample presents even weaker XRD peaks indicative of  $MnO_x$  and VMT, and no additional crystal phases are observed. Here, the coexistence of manganese and iron oxides enhances dispersion, and consequently reduces the crystallinity, indicating the presence of strong interactions between these two metal oxides [38].

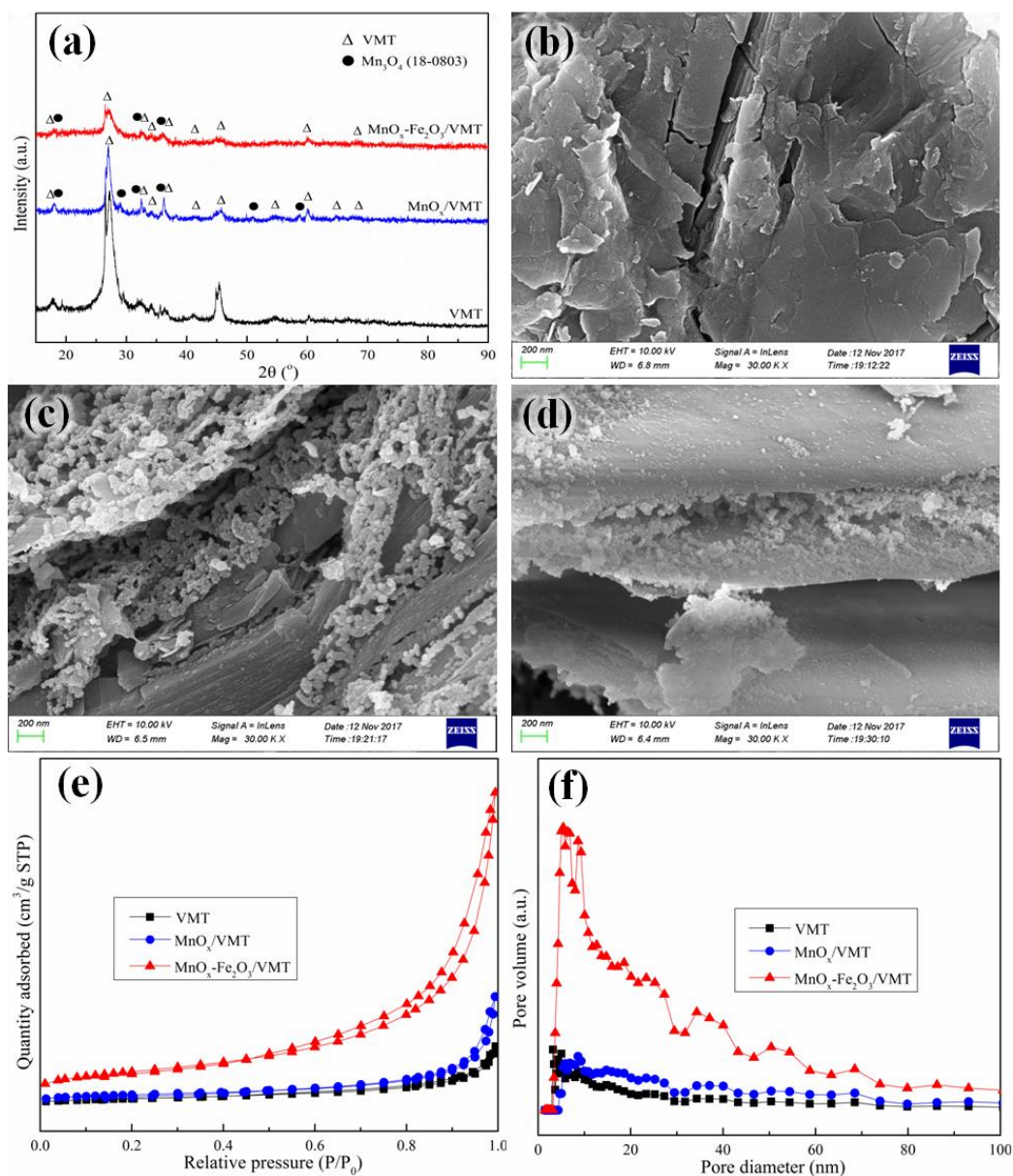


**Figure 2.** XRD patterns (a); N<sub>2</sub> isotherms (b) and pore diameter distribution curves (c); scanning electron microscopy (SEM) images (d–f) of the VMT support and MnO<sub>x</sub>/VMT and MnO<sub>x</sub>-Fe<sub>2</sub>O<sub>3</sub>/VMT catalyst samples.

Figure 2b–d present SEM micrographs indicative of the morphologies of the VMT support and as-prepared MnO<sub>x</sub>/VMT and MnO<sub>x</sub>-Fe<sub>2</sub>O<sub>3</sub>/VMT catalysts, respectively. We note the distinct layered structure of the VMT support, and that the layer surfaces are very smooth, without obvious pores or wrinkles. After impregnation, the MnO<sub>x</sub>/VMT catalyst exhibits a distribution of irregular loose particles, and the layer surfaces of the VMT support appear to be very rough (Figure 2c), indicating the formation of many new channels on the VMT surfaces. However, the sizes of the irregular loose particles of the MnO<sub>x</sub>-Fe<sub>2</sub>O<sub>3</sub>/VMT catalyst are substantially decreased. These results explain the reason for the increased surface area and decreased pore diameter of the MnO<sub>x</sub>-Fe<sub>2</sub>O<sub>3</sub>/VMT catalyst relative to those of the MnO<sub>x</sub>/VMT catalyst.

The N<sub>2</sub> adsorption-desorption isotherm plots and the corresponding BJH pore size distribution curves of the VMT support and as-prepared MnO<sub>x</sub>/VMT and MnO<sub>x</sub>-Fe<sub>2</sub>O<sub>3</sub>/VMT catalyst samples are presented in Figure 2e,f, respectively. From Figure 2e, we note the presence of well-defined type II hysteresis loops with sloping adsorption branches for all samples, which is particularly pronounced for the MnO<sub>x</sub>-Fe<sub>2</sub>O<sub>3</sub>/VMT catalyst. From Figure 2f, we note that both catalyst samples exhibit three narrow peaks in the pore diameter range of 2–10 nm. The textural data for all samples are listed in Table 1. From the table, we find that the impregnation of 20 wt% Mn more than doubled the BET surface area of the MnO<sub>x</sub>/VMT catalyst sample relative to that of the VMT support, but, surprisingly, the pore diameter decreased by about 30%. Moreover, the impregnation of 20 wt% Mn and 5 wt% Fe further increased the BET surface area of the MnO<sub>x</sub>-Fe<sub>2</sub>O<sub>3</sub>/VMT catalyst sample by a factor greater than 3 relative to the MnO<sub>x</sub>/VMT catalyst sample, while the pore diameter further decreased by about 12%. These results indicate that the doping of second metal can change the surface structure of the MnO<sub>x</sub>-Fe<sub>2</sub>O<sub>3</sub>/VMT catalyst [39], and the calcination subsequent to impregnation may have formed additional channels in the surfaces of the VMT support. A high BET surface area is beneficial toward increasing the number of active sites of a catalyst and, thus, provides an increased NO conversion.

**Table 1.** Physical properties of VMT support and catalyst samples.

| Samples  | BET Surface Area (m <sup>2</sup> /g) | Pore Volume (cm <sup>3</sup> /g) | Pore Diameter (nm) |
|--|--------------------------------------|----------------------------------|--------------------|
| VMT support  | 2.9                                  | 0.02                             | 26.2               |
| MnO <sub>x</sub> /VMT                                      | 6.7                                  | 0.03                             | 18.4               |
| MnO <sub>x</sub> -Fe <sub>2</sub> O <sub>3</sub> /VMT      | 21.9                                 | 0.09                             | 16.2               |
| MnO <sub>x</sub> -Fe <sub>2</sub> O <sub>3</sub> /VMT MHCs | 15.4                                 | 0.07                             | 17.9               |

The XPS spectra of the as-prepared MnO<sub>x</sub>/VMT and MnO<sub>x</sub>-Fe<sub>2</sub>O<sub>3</sub>/VMT catalysts are shown in Figure 3, and their principle surface compositions obtained from the fitted spectra in Figure 3b–d are listed in Table 2. Sharp photoelectron peaks are observed in Figure 3a for Fe, Mn, O, and C elements with binding energies of 712.1 eV (Fe 2p<sub>3/2</sub>), 642.1 eV (Mn 2p<sub>3/2</sub>), 532.1 eV (O 1s), and 284.1 eV (C 1s), respectively. We note that the XPS spectrum obtained for the MnO<sub>x</sub>/VMT catalyst also exhibits a small peak indicative of Fe because the VMT support material naturally contains a small concentration of Fe. The Fe 2p, Mn 2p, and O 1s spectra of the catalyst samples are individually discussed in detail below.

**Table 2.** Surface compositions of representative catalyst samples obtained by XPS analysis.

| Samples   | Mn <sup>4+</sup> /Mn <sub>total</sub> (%) | O <sub>ads</sub> /O <sub>total</sub> (%) | Fe <sup>3+</sup> /Fe <sub>total</sub> (%) |
|---|---|--|---|
| MnO <sub>x</sub> /VMT                                 | 26.3                                      | 38.5                                     | 51.5                                      |
| MnO <sub>x</sub> -Fe <sub>2</sub> O <sub>3</sub> /VMT | 35.9                                      | 46.0                                     | 59.1                                      |

As shown in Figure 3b, the Mn 2p spectra include two main peaks at binding energies of 653.8 ± 0.4 eV and 641.9 ± 0.4 eV, which are assigned to Mn 2p<sub>3/2</sub> and Mn 2p<sub>1/2</sub> electron states,

respectively. To identify the specific Mn species of each sample, the Mn 2p<sub>3/2</sub> peak was deconvoluted into three peaks, corresponding to Mn<sup>2+</sup> (641.0 ± 0.4 eV), Mn<sup>3+</sup> (642.1 ± 0.4 eV), and Mn<sup>4+</sup> (643.5 ± 0.4 eV), respectively [40]. The percentage of Mn atoms in the Mn<sup>4+</sup> state listed in Table 2 was then determined as the area under the curve representative of Mn<sup>4+</sup> relative to the total area under the Mn 2p<sub>3/2</sub> curve. These values are indicative of the molar concentration of MnO<sub>2</sub> relative to all MnO<sub>x</sub> on the surfaces of the MnO<sub>x</sub>-Fe<sub>2</sub>O<sub>3</sub>/VMT and MnO<sub>x</sub>/VMT catalysts. We note that the Mn<sup>4+</sup> percentage increased by about 37% from the MnO<sub>x</sub>/VMT catalyst to the MnO<sub>x</sub>-Fe<sub>2</sub>O<sub>3</sub>/VMT catalyst. This indicates that the addition of Fe facilitates the conversion of MnO<sub>x</sub> to MnO<sub>2</sub> on the catalyst surface. It has been reported [41–43] that the NO conversion capability of pure manganese oxides can be ranked as MnO<sub>2</sub> > Mn<sub>5</sub>O<sub>8</sub> > Mn<sub>2</sub>O<sub>3</sub> > Mn<sub>3</sub>O<sub>4</sub>. In addition, it has been reported that a greater concentration of MnO<sub>2</sub> on the catalyst surface promotes the SCR reaction [44]. Therefore, it can be expected that the MnO<sub>x</sub>-Fe<sub>2</sub>O<sub>3</sub>/VMT catalyst will provide an improved NO conversion relative to that of the MnO<sub>x</sub>/VMT catalyst.

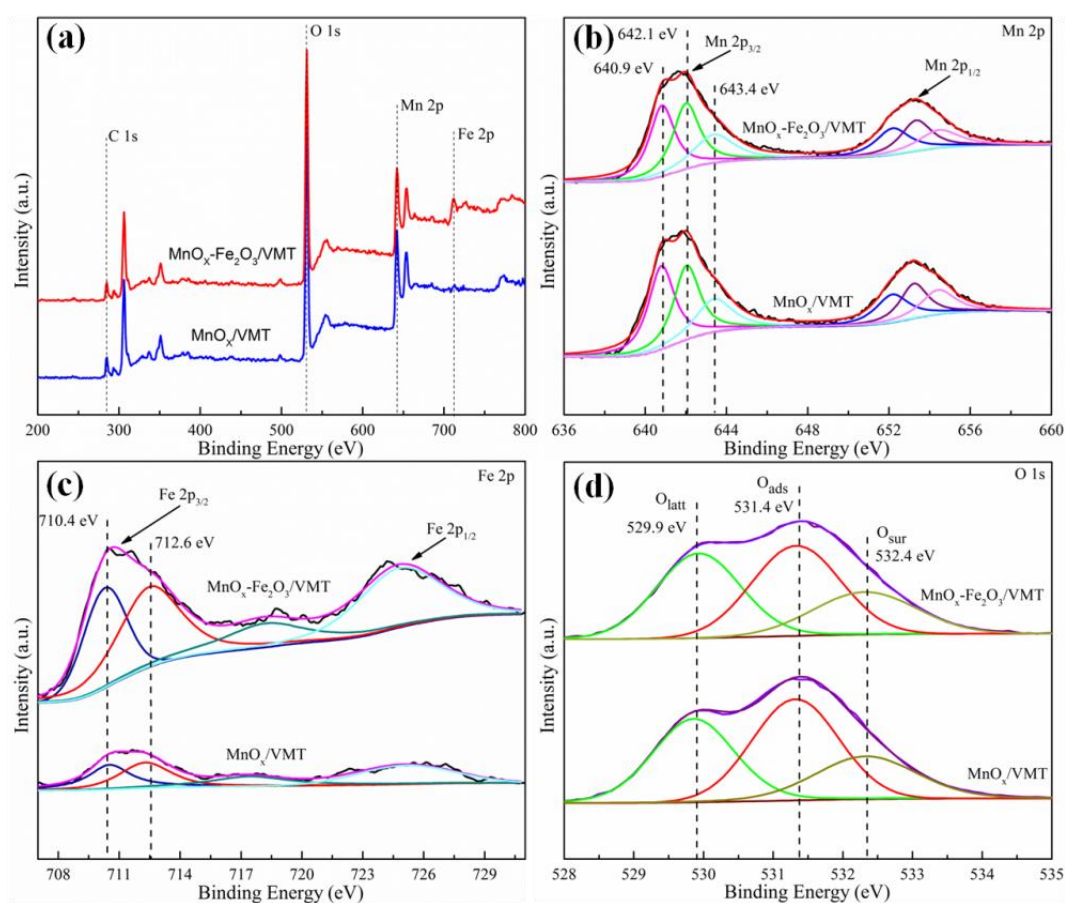


**Figure 3.** XPS survey spectra (a); Mn 2p spectra (b); Fe 2p spectra (c); O 1s spectra (d) of MnO<sub>x</sub>/VMT and MnO<sub>x</sub>-Fe<sub>2</sub>O<sub>3</sub>/VMT catalyst samples.

The Fe 2p spectra presented in Figure 3c exhibit electron binding energy peak values for Fe 2p<sub>3/2</sub> and Fe 2p<sub>1/2</sub> states, and a satellite peak of 710.7, 725.0, and 718.6 eV, respectively. The satellite peak energy corresponds well with that reported for Fe<sub>2</sub>O<sub>3</sub> [45]. The Fe 2p<sub>3/2</sub> peak was deconvoluted into two components with peaks at 710.4 eV and 712.6 eV indicative of Fe<sup>2+</sup> and Fe<sup>3+</sup> phases [46], respectively. The results indicate that the percentage of Fe atoms in the Fe<sup>3+</sup> state listed in Table 2 are about 13% less in the VMT support of the MnO<sub>x</sub>/VMT catalyst than that of the MnO<sub>x</sub>-Fe<sub>2</sub>O<sub>3</sub>/VMT catalyst. According to a past study [47], Fe<sup>3+</sup> sites may facilitate the reduction of NO<sub>x</sub> at low temperature. Thus, the MnO<sub>x</sub>-Fe<sub>2</sub>O<sub>3</sub>/VMT catalyst can be expected to provide a slightly better low-temperature activity than that of the MnO<sub>x</sub>/VMT catalyst.

As shown in Figure 3d the O 1s peaks of the MnO<sub>x</sub>/VMT and MnO<sub>x</sub>-Fe<sub>2</sub>O<sub>3</sub>/VMT catalysts at 528–535 eV were deconvoluted into three peaks, denoted as O<sub>latt</sub> (529.9 eV), O<sub>ads</sub> (531.4 eV), and O<sub>sur</sub>

(532.4 eV), which are attributed to O atoms bonded with metal cations, in adsorbed water, and in surface hydroxyl groups, respectively [48]. It has been widely reported that oxygen in the gas phase can be activated by oxygen vacancies on the surface of SCR catalysts. Therefore, the relative abundance of  $O_{\text{ads}}$  is of particular interest because an increased percentage of  $O_{\text{ads}}$  can promote the oxidation of NO to  $\text{NO}_2$ , and enhance the SCR performance at low temperature through a rapid  $\text{NH}_3$ -SCR route [49,50]. As shown in Table 2, the ratio of  $O_{\text{ads}}/O_{\text{total}}$  on the surface of the  $\text{MnO}_x\text{-Fe}_2\text{O}_3/\text{VMT}$  catalyst is about 19% greater than that for the  $\text{MnO}_x/\text{VMT}$  catalyst. As a result, we can expect this factor to further enhance the low-temperature activity of the  $\text{MnO}_x\text{-Fe}_2\text{O}_3/\text{VMT}$  catalyst relative to that of the  $\text{MnO}_x/\text{VMT}$  catalyst.

The results of  $\text{H}_2$ -TPR testing are presented in Figure 4 for the VMT support and the as-prepared  $\text{MnO}_x/\text{VMT}$  and  $\text{MnO}_x\text{-Fe}_2\text{O}_3/\text{VMT}$  catalysts. We note that several peaks are observable for all samples within the temperature range of 200–800 °C. The  $\text{H}_2$ -TPR curve for the VMT support includes only two peaks, with a reduction peak attributed to  $\text{Fe}_2\text{O}_3 \rightarrow \text{Fe}_3\text{O}_4$  at 274 °C, and a second peak located at 688 °C that may be attributed to  $\text{Fe}_3\text{O}_4 \rightarrow \text{FeO}$  [51]. Compared with the VMT support curve, two new reduction peaks are observed in the  $\text{H}_2$ -TPR curve for the  $\text{MnO}_x/\text{VMT}$  catalyst due to the addition of Mn. From previous studies [52], the reduction peaks of  $\text{MnO}_x$  can be assigned to the reduction processes of  $\text{MnO}_2$  via  $\text{Mn}_2\text{O}_3$  to  $\text{MnO}$ . Here, the first peak observed at 269 °C can be attributed to the  $\text{MnO}_2 \rightarrow \text{Mn}_2\text{O}_3$  reduction transition, while the peak at 469 °C can be attributed to  $\text{Mn}_2\text{O}_3 \rightarrow \text{MnO}$  [53]. Therefore, because the  $\text{MnO}_x/\text{VMT}$  catalyst includes  $\text{Fe}_2\text{O}_3$  in the support, the peak centered at 269 °C can be attributed to both  $\text{Fe}_2\text{O}_3 \rightarrow \text{Fe}_3\text{O}_4$  and  $\text{MnO}_2 \rightarrow \text{Mn}_2\text{O}_3$ . Meanwhile, the third peak for the  $\text{MnO}_x/\text{VMT}$  sample located at 608 °C can be attributed to  $\text{Fe}_3\text{O}_4 \rightarrow \text{FeO}$ , and the fourth peak located at 742 °C can be attributed to  $\text{FeO} \rightarrow \text{Fe}$  [54]. The  $\text{H}_2$ -TPR curve for the  $\text{MnO}_x\text{-Fe}_2\text{O}_3/\text{VMT}$  catalyst exhibited similar reduction peaks above 260 °C, but which were shifted to lower temperatures relative to those for the  $\text{MnO}_x/\text{VMT}$  catalyst, suggesting that the Fe and Mn species in the  $\text{MnO}_x\text{-Fe}_2\text{O}_3/\text{VMT}$  catalyst were more easily reduced. This can be ascribed to the previously discussed synergistic effect between Mn and Fe, which could effectively promote the redox properties of the  $\text{MnO}_x\text{-Fe}_2\text{O}_3/\text{VMT}$  catalyst and improve its catalytic activity.

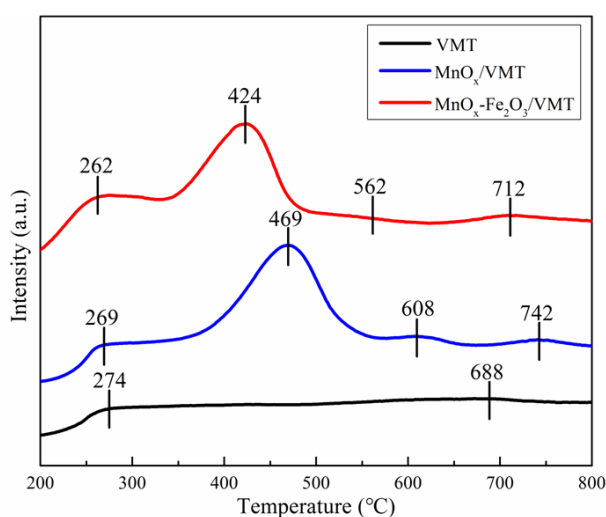


**Figure 4.**  $\text{H}_2$ -TPR curves of the VMT support and  $\text{MnO}_x/\text{VMT}$  and  $\text{MnO}_x\text{-Fe}_2\text{O}_3/\text{VMT}$  catalyst samples.

A photograph of the as-prepared  $\text{MnO}_x\text{-Fe}_2\text{O}_3/\text{VMT}$  MHCs is shown in Figure 5a. The macrostructure of the  $\text{MnO}_x\text{-Fe}_2\text{O}_3/\text{VMT}$  MHCs is important for promoting catalytic activity in industrial applications, and their primary physical properties have significant effects on their mechanical and catalytic performances. The SEM micrograph of an as-prepared  $\text{MnO}_x\text{-Fe}_2\text{O}_3/\text{VMT}$  MHCs in Figure 5b shows that the glass fibers were uniformly distributed throughout the  $\text{MnO}_x\text{-Fe}_2\text{O}_3/\text{VMT}$  MHCs, which can be expected to provide enhanced mechanical strength. The XRD pattern of a representative  $\text{MnO}_x\text{-Fe}_2\text{O}_3/\text{VMT}$  MHCs is shown in Figure 5c. In contrast with the XRD results for the  $\text{MnO}_x\text{-Fe}_2\text{O}_3/\text{VMT}$  powdered catalyst (Figure 2a), the bentonite content in the MHCs,

which has a large proportion of SiO<sub>2</sub>, yields a sharp peak attributable to SiO<sub>2</sub> (PDF#27-0605) at 21.6°. In addition, two sharp peaks attributable to carbon (PDF#41-1487) are observed at 26.4° and 54.5° owing to the decomposition of the organic additives. Figure 5d presents the N<sub>2</sub> isotherms and corresponding pore size distribution curve (inset) of a MnO<sub>x</sub>-Fe<sub>2</sub>O<sub>3</sub>/VMT MHCs, and the corresponding textural data are listed Table 1. Here, we note that, while the BET surface area and pore volume of the MnO<sub>x</sub>-Fe<sub>2</sub>O<sub>3</sub>/VMT MHCs were less than those of its powdered counterpart, the average pore diameter was increased by around 10%. The porous texture of the MnO<sub>x</sub>-Fe<sub>2</sub>O<sub>3</sub>/VMT MHCs can be expected to play a significant role in the SCR of NO<sub>x</sub> owing to an enhanced transportation and adsorption of reactant gases.

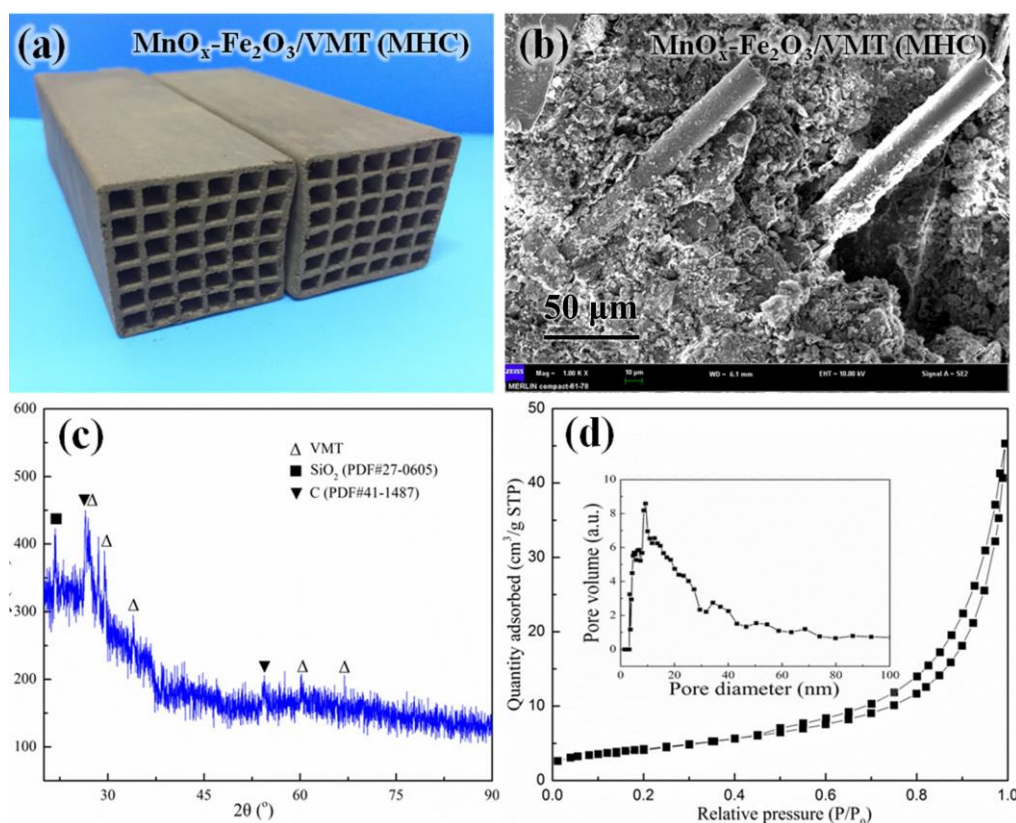


**Figure 5.** MnO<sub>x</sub>-Fe<sub>2</sub>O<sub>3</sub>/VMT MHCs: (a) photograph of as-prepared MHCs; (b) SEM image; (c) XRD pattern; (d) N<sub>2</sub> isotherms and corresponding pore size distribution curve (inset).

The NO conversion of MnO<sub>x</sub>-Fe<sub>2</sub>O<sub>3</sub>/VMT MHCs at different GHSV values is shown as a function of reaction temperature in Figure 6a. We note that the NO conversion decreased with an increasing GHSV from 4000 h<sup>-1</sup> to 8000 h<sup>-1</sup>. The temperature region of highest activity was between 150 °C and 200 °C, and the NO conversion attained a maximum value greater than 98% with GHSV = 4000 h<sup>-1</sup>. Meanwhile, the MnO<sub>x</sub>-Fe<sub>2</sub>O<sub>3</sub>/VMT MHCs exhibited an excellent NO conversion of 39.2% and 53.4% at 20 °C and 50 °C, respectively, with GHSV = 4000 h<sup>-1</sup>. The cycling stabilities of MnO<sub>x</sub>-Fe<sub>2</sub>O<sub>3</sub>/VMT MHCs are presented in Figure 6b at various temperatures with different GHSV values. We note that the NO conversion was stable, with no significant changes over a full 10 h of testing. We also find that the MnO<sub>x</sub>-Fe<sub>2</sub>O<sub>3</sub>/VMT MHCs provided excellent NO conversion values of 98.6% and 85.8% at 150 °C and 100 °C, respectively, with GHSV = 4000 h<sup>-1</sup>. The results obtained are comparable to those reported in the literature (Figure 6c). Thus, a NO conversion of 92% at 500 °C has been reported for WO<sub>3</sub>-TiO<sub>2</sub> (GHSV of 11,000 h<sup>-1</sup>) [55], a conversion of 98% at 400 °C was reached by V<sub>2</sub>O<sub>5</sub>-MoO<sub>3</sub>/TiO<sub>2</sub> (GHSV of 6000 h<sup>-1</sup>) [56]. A TiO<sub>2</sub> catalyst showed a conversion of 80% at 300 °C (GHSV of 25,000 h<sup>-1</sup>) [57], 75% at 250 °C for a V<sub>2</sub>O<sub>5</sub>-WO<sub>3</sub>/TiO<sub>2</sub> catalyst (GHSV of 27,000 h<sup>-1</sup>) [58], and 90% at 160 °C for a Cr-V/TiO<sub>2</sub> catalyst (GHSV of 4000 h<sup>-1</sup>) [59]. Even at GHSV = 2000 h<sup>-1</sup>, the MnO<sub>x</sub>-Fe<sub>2</sub>O<sub>3</sub>/VMT MHCs provided an NO conversion of 79.1% at 50 °C. Surprisingly, the MHCs exhibited excellent NO

conversion values of 62.2% and 50.2% with GHSV = 1000 h<sup>-1</sup> and 2000 h<sup>-1</sup>, respectively, at 20 °C. The excellent SCR performance obtained for the proposed MnO<sub>x</sub>-Fe<sub>2</sub>O<sub>3</sub>/VMT MHCs will strongly contribute to low-temperature De-NO<sub>x</sub> processes, and suggests that even room temperature processes are feasible.

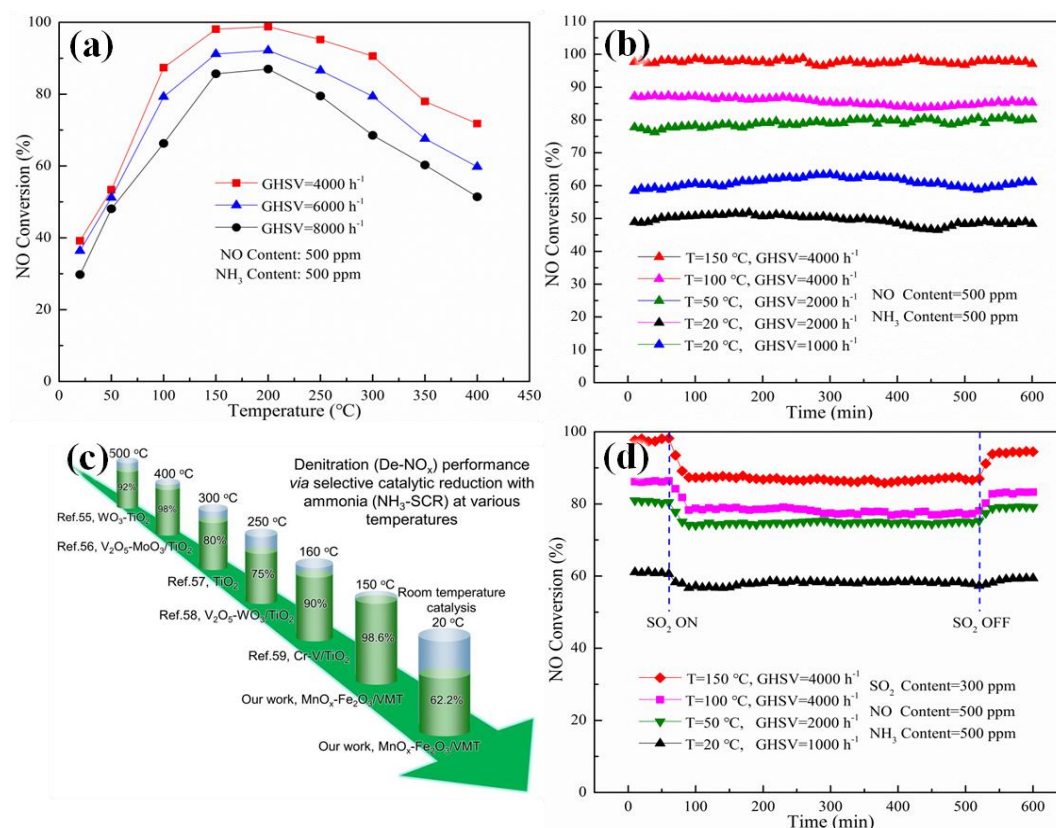


**Figure 6.** Catalytic activity of MnO<sub>x</sub>-Fe<sub>2</sub>O<sub>3</sub>/VMT MHCs: (a) NO conversion; (b) cycling stabilities; (c) Comparison of pervious reported activity of various MHCs for NH<sub>3</sub>-SCR; (d) SO<sub>2</sub> resistance at various temperatures with different GHSV.

The impact of SO<sub>2</sub> on the cycling performance of MnO<sub>x</sub>-Fe<sub>2</sub>O<sub>3</sub>/VMT MHCs at different temperatures and GHSV values is shown in Figure 6d. After the first 1 h of testing when 300 ppm SO<sub>2</sub> was introduced into the reaction gas, we note that the extent to which the NO conversion decreased was only slight at 20 °C (GHSV = 1000 h<sup>-1</sup>), but increased with increasing temperature from 50 °C (GHSV = 2000 h<sup>-1</sup>) to 150 °C (GHSV = 4000 h<sup>-1</sup>). This is because the crystallization temperature of sulfate is greater than 40 °C. We also note that the NO conversion of the MnO<sub>x</sub>-Fe<sub>2</sub>O<sub>3</sub>/VMT MHCs was stable over the entire period of SO<sub>2</sub> addition, which indicates good SO<sub>2</sub> resistance. However, the NO conversion values obtained under all conditions did not recover to their original values when the addition of SO<sub>2</sub> was discontinued. These results suggest that the decreased activity of the MHCs was not due to the competitive adsorption of SO<sub>2</sub>, but because of the formation of sulfates covering the active sites of the catalysts [60].

### 3. Materials and Methods

#### 3.1. Catalysts Preparation

##### 3.1.1. Preparation of MnO<sub>x</sub>/VMT and MnO<sub>x</sub>-Fe<sub>2</sub>O<sub>3</sub>/VMT Catalysts

Vermiculite supports were prepared by a microwave method as follows. The raw VMT (Xinjiang Yuli Xinlong Vermiculite Co., Ltd., Korla, China) was washed with water until no trace of foreign material was observable under visual inspection, and then dried in an oven at 100 °C. Finally, the

washed VMT was placed in a 500 mL beaker and expanded in a microwave. The VMT was collected and placed in a sealed container, and then crushed prior to use. All the catalysts were prepared by the impregnation method. We completely dissolved  $\text{Mn}(\text{CH}_3\text{COO})_2 \cdot 4\text{H}_2\text{O}$  in water under stirring in an appropriate ratio to the VMT content (i.e., 20 wt% Mn). We added the VMT powder, and continued stirring for 10 h. The sample was dried in air at 100 °C for 12 h, and then crushed and sieved in an 80–100 mesh sieve. Finally, the sample was calcined in air at 500 °C for 5 h. We prepared  $\text{MnO}_x\text{-Fe}_2\text{O}_3/\text{VMT}$  catalysts by an equivalent method using  $\text{Mn}(\text{CH}_3\text{COO})_2 \cdot 4\text{H}_2\text{O}$  and  $\text{Fe}(\text{NO}_3)_3 \cdot 9\text{H}_2\text{O}$  (20 wt% Mn-5 wt% Fe relative to VMT).

### 3.1.2. Preparation of $\text{MnO}_x\text{-Fe}_2\text{O}_3/\text{VMT}$ Monolithic Honeycomb Catalysts

We synthesized  $\text{MnO}_x\text{-Fe}_2\text{O}_3/\text{VMT}$  MHCs by an extrusion molding method. The powdered  $\text{MnO}_x\text{-Fe}_2\text{O}_3/\text{VMT}$  catalyst was dry mixed with 10 wt% bentonite and 3 wt% carboxy methyl cellulose (CMC) in a blender mixer. The materials in the blender mixer were then wet mixed with 10 wt% glycerin, followed by a sufficient amount of water to ensure an appropriate viscosity for extrusion. The resulting mixture was kneaded by hand for 30 min until achieving a uniform consistency. The sample was subjected to vacuum de-airing and aged for 24 h to increase the plasticity. The aged sample was molded by an extruding machine to obtain a monolithic honeycomb structure. The honeycomb sample was dried at 70 °C in air for 12 h in a muffle furnace, further dried at 100 °C for 12 h, and then calcined at 500 °C for 5 h. The rate of temperature increase was 1 °C/min for all the above steps. The mold size was 3.3 cm × 3.3 cm with 36 channels (i.e., 6 × 6 cells).

### 3.2. Catalyst Characterization

The morphologies of the powder catalysts and MHCs were characterized by scanning electron microscopy (SEM; Hitachi S-4300, Hitachi Limited, Tokyo, Japan). A BET apparatus (Micromeritics ASAP 2020, Micromeritics Instrument Ltd., Norcross, GA, USA) was employed to measure the Brunauer-Emmett-Teller (BET) specific surface area and Barrett-Joyner-Halenda (BJH) pore structure of the powder catalysts and MHCs. The samples were degassed in vacuum at 200 °C for 4 h prior to measurement. The total pore volume was calculated from the volume of nitrogen adsorbed at  $P/P_0 = 0.99$ . Powder X-ray diffraction (XRD) patterns were recorded on a Bruker D8 Advance X-ray diffractometer (Bruker Biosciences Corporation, Billerica, MA, USA) with  $\text{Cu K}\alpha$  radiation ( $\lambda = 1.5406 \text{ \AA}$ ) operated at 40 kV and 40 mA. X-ray photoelectron spectroscopy (XPS) data were obtained with an AMICUS/ESCA 3400 electron spectrometer from Kratos Analytical (Manchester, UK) using  $\text{Mg K}\alpha$  radiation (20 mA, 12 kV). Binding energies were referenced to the C 1s line at 284.8 eV for adventitious carbon. We conducted  $\text{H}_2$  temperature programmed reduction ( $\text{H}_2\text{-TPR}$ ) testing to analyze the redox properties of the catalysts using a Micromeritics ChemiSorb 2720TPx system (Micromeritics Instrument Ltd., Norcross, GA, USA) in a temperature range of 20 °C to 800 °C at a rate of 10 °C/min with a gas (10 vol%  $\text{H}_2$  relative to Ar) flow rate of 40 mL/min, and then retained for 20 min at 800 °C.

### 3.3. Activity Measurement

We prepared  $\text{MnO}_x/\text{VMT}$  and  $\text{MnO}_x\text{-Fe}_2\text{O}_3/\text{VMT}$  catalytic activity studies using a fixed bed microreactor. The reactor was composed of a stainless steel tube with a 10.0 mm inner diameter. Prior to conducting the experiments, quartz sand and quartz wool were placed inside the reaction tube to ensure contact between the powdered catalysts and the thermocouple. The typical composition of the simulated flue gas was 500 ppm NO (denoted as  $[\text{NO}]_{\text{in}}$ ), 500 ppm  $\text{NH}_3$  (denoted as  $[\text{NH}_3]_{\text{in}}$ ), and 5 vol%  $\text{O}_2$  with  $\text{N}_2$  as the balance gas. The total volume flow was 100 mL/min, representing a GHSV of 30,000  $\text{h}^{-1}$ . The catalytic activity of the powdered catalysts was evaluated in the temperature range of 20 °C to 400 °C during testing according to the exiting concentrations of NO (denoted as  $[\text{NO}]_{\text{out}}$ ) and  $\text{NH}_3$  (denoted as  $[\text{NH}_3]_{\text{out}}$ ) determined by Fourier transform infrared (FTIR) spectroscopy (Nicolet IS10, Thermo Fisher Scientific, Waltham, MA, USA). The NO conversion ( $[\text{NO}]_{\text{conversion}}$ ) and  $\text{N}_2$  selectivity ( $[\text{N}_2]_{\text{selectivity}}$ ) were calculated using the following equations:

$$[\text{NO}]_{\text{conversion}} = \frac{[\text{NO}]_{\text{in}} - [\text{NO}]_{\text{out}}}{[\text{NO}]_{\text{in}}} \times 100\% \quad (1)$$

$$[\text{N}_2]_{\text{selectivity}} = \left[ 1 - \frac{[\text{NO}_2]_{\text{out}} + 2[\text{N}_2\text{O}]_{\text{out}}}{[\text{NO}]_{\text{in}} - [\text{NO}]_{\text{out}} + [\text{NH}_3]_{\text{in}} - [\text{NH}_3]_{\text{out}}} \right] \times 100\% \quad (2)$$

The catalytic performance of MnO<sub>x</sub>-Fe<sub>2</sub>O<sub>3</sub>/VMT MHCs was evaluated using a similar fixed bed microreactor composed of a quartz tube with a 5.0 cm inner diameter. The simulated flue gas was composed of 500 ppm NO and 500 ppm NH<sub>3</sub> with air as the balance gas. Prior to testing, each MHCs sample was placed in the reaction tube, and then exposed to the simulated flue gas for 1 h to eliminate the influence of adsorption on the catalysts. Then, [NO]<sub>out</sub> was measured online using a flue gas analyzer (QUINTOX-KM9106, Kane International, New York, NY, USA), and [NO]<sub>conversion</sub> was calculated using Equation (1). Unless otherwise stated here, all other conditions were equivalent to the conditions employed for powdered catalysts.

#### 4. Conclusions

This paper presented the successful preparation of MnO<sub>x</sub>-Fe<sub>2</sub>O<sub>3</sub>/VMT catalysts with a layered structure by an impregnation method for the first time. The as-prepared MnO<sub>x</sub>-Fe<sub>2</sub>O<sub>3</sub>/VMT catalysts exhibited high NO conversion and N<sub>2</sub> selectivity for the NH<sub>3</sub>-SCR of NO in the temperature range of 20–200 °C. The catalysts provided an excellent NO conversion of 96.5% at 200 °C with GHSV = 30,000 h<sup>-1</sup> and an NO concentration of 500 ppm. Compared with VMT and MnO<sub>x</sub>/VMT catalysts, the results of extensive characterization indicated that the high catalytic activity of the MnO<sub>x</sub>-Fe<sub>2</sub>O<sub>3</sub>/VMT catalysts can be attributed to a number of advantageous properties, such as a large specific surface area, high ratios of Mn<sup>4+</sup>/Mn<sub>total</sub> and Fe<sup>3+</sup>/Fe<sub>total</sub>, and easily reduced Mn species. In addition, the MnO<sub>x</sub>-Fe<sub>2</sub>O<sub>3</sub>/VMT powdered catalyst was successfully employed to form MHCs by an extrusion method. The as-prepared MnO<sub>x</sub>-Fe<sub>2</sub>O<sub>3</sub>/VMT MHCs provided an NO conversion of 98.6% at 150 °C with GHSV = 4000 h<sup>-1</sup>. Moreover, the MHCs presented excellent De-NO<sub>x</sub> performance at low temperature, obtaining an NO conversion of 62.2% at 20 °C with GHSV = 1000 h<sup>-1</sup>. Furthermore, the MnO<sub>x</sub>-Fe<sub>2</sub>O<sub>3</sub>/VMT MHCs also provided excellent cycling stability, and maintained comparable NO conversion values even after 10 h. Finally, the MnO<sub>x</sub>-Fe<sub>2</sub>O<sub>3</sub>/VMT MHCs demonstrated excellent SO<sub>2</sub> resistance at low temperature (particularly at room temperature). Therefore, the prepared MnO<sub>x</sub>-Fe<sub>2</sub>O<sub>3</sub>/VMT MHCs offer considerable potential for low or even room temperature De-NO<sub>x</sub> applications in stationary stack source emissions.

**Acknowledgments:** The work was supported by National High Technology Research and Development Program of China (863 program) (no. 2015AA03A401), Program for Changjiang Scholars and Innovative Research Team in University (no. IRT\_15R46) and the Program of Science and Technology Innovation Team in Bingtuan (no. 2015BD003).

**Author Contributions:** F.Y. and B.D. designed and administered the experiments. K.Z. performed experiments. M.Z., J.D., X.W., and J.Z. collected and analyzed data. All authors discussed the data and wrote the manuscript.

**Conflicts of Interest:** The authors declare no conflicts of interests.

#### References

1. Cai, S.; Liu, J.; Zha, K.; Li, H.; Shi, L.; Zhang, D. A general strategy for the in situ decoration of porous Mn-Co bi-metal oxides on metal mesh/foam for high performance de-NO<sub>x</sub> monolith catalysts. *Nanoscale* **2017**, *9*, 5648–5657.
2. Boningari, T.; Smirniotis, P.G. Impact of nitrogen oxides on the environment and human health: Mn-based materials for the NO<sub>x</sub> abatement. *Curr. Opin. Chem. Eng.* **2016**, *13*, 133–141.
3. Li, J.H.; Chang, H.Z.; Ma, L.; Hao, J.M.; Yang, R.T. Low-temperature selective catalytic reduction of NO<sub>x</sub> with NH<sub>3</sub> over metal oxide and zeolite catalysts—A review. *Catal. Today* **2011**, *175*, 147–156.
4. Zhu, Y.; Chen, B.; Zhao, R.; Zhao, Q.; Gies, H.; Xiao, F.; Vos, D.E.D.; Yokoi, T.; Bao, X.; Kolb, U.; et al. Fe-doped Beta Zeolite from Organotemplate-free Synthesis for NH<sub>3</sub>-SCR of NO<sub>x</sub>. *Catal. Sci. Technol.* **2016**, *6*, 6581–6592.

5. Liu, C.; Shi, J.W.; Niu, C. Manganese oxide-based catalysts for low-temperature selective catalytic reduction of NO<sub>x</sub> with NH<sub>3</sub>: A review. *Appl. Catal. A Gen.* **2016**, *522*, 54–69.
6. Long, R.Q.; Yang, R.T.; Chang, R. Low temperature selective catalytic reduction (SCR) of NO with NH<sub>3</sub> over Fe-Mn based catalysts. *Chem. Commun.* **2012**, *5*, 452–453.
7. Boningari, T.; Pappas, D.K.; Ettireddy, P.R.; Kotrba, A.; Smirniotis, P.G. Influence of SiO<sub>2</sub> on M/TiO<sub>2</sub> (M = Cu, Mn, and Ce) formulations for low-temperature selective catalytic reduction of NO<sub>x</sub> with NH<sub>3</sub>: Surface properties and key components in relation to the activity of NO<sub>x</sub> reduction. *Ind. Eng. Chem. Res.* **2015**, *54*, 2261–2273.
8. Chen, Z.; Wang, F.; Li, H.; Yang, Q.; Wang, L.F.; Li, X.H. Low-Temperature Selective Catalytic Reduction of NO<sub>x</sub> with NH<sub>3</sub> over Fe-Mn Mixed-Oxide Catalysts Containing Fe<sub>3</sub>Mn<sub>3</sub>O<sub>8</sub> Phase. *Ind. Eng. Chem. Res.* **2012**, *51*, 202–212.
9. Li, R.; Li, Z.B.; Chen, L.Q.; Dong, Y.L.; Ma, S.B.; Yuan, F.L.; Zhu, Y.J. Synthesis of MnNi-SAPO-34 by a one-pot hydrothermal method and its excellent performance for the selective catalytic reduction of NO by NH<sub>3</sub>. *Catal. Sci. Technol.* **2017**, *7*, 4989–4995.
10. Lou, X.; Liu, P.; Li, J.; Li, Z.; He, K. Effects of calcination temperature on Mn species and catalytic activities of Mn/ZSM-5 catalyst for selective catalytic reduction of NO with ammonia. *Appl. Sur. Sci.* **2014**, *307*, 382–387.
11. Yu, C.; Dong, L.; Feng, C.; Liu, X.; Huang, B. Low-temperature SCR of NO<sub>x</sub> by NH<sub>3</sub> over MnO<sub>x</sub>/SAPO-34 prepared by two different methods: A comparative study. *Environ. Technol.* **2017**, *38*, 1030–1042.
12. Liu, J.; Zhang, K.; Si, M.; Lian, J.H.; Liu, L.S.; Gou, X. Experimental Research on Catalysts of V<sub>2</sub>O<sub>5</sub>/AC and V<sub>2</sub>O<sub>5</sub>/CNTs for Low Temperature SCR Denitrification. *Appl. Mech. Mater.* **2014**, *694*, 478–483.
13. Lu, X.; Zheng, Y.; Zhang, Y.; Qiu, H. Low-temperature selective catalytic reduction of NO over carbon nanotubes supported MnO<sub>2</sub> fabricated by co-precipitation method. *Micro Nano Lett.* **2015**, *10*, 666–669.
14. Lin, F.; Wu, X.; Liu, S.; Weng, D.; Huang, Y. Preparation of MnO<sub>x</sub>-CeO<sub>2</sub>-Al<sub>2</sub>O<sub>3</sub> mixed oxides for NO<sub>x</sub>-assisted soot oxidation: Activity, structure and thermal stability. *Chem. Eng. J.* **2013**, *226*, 105–112.
15. Jin, R.; Liu, Y.; Wu, Z.; Wang, H.; Gu, T. Low-temperature selective catalytic reduction of NO with NH<sub>3</sub> over MnCe oxides supported on TiO<sub>2</sub> and Al<sub>2</sub>O<sub>3</sub>: A comparative study. *Chemosphere* **2010**, *78*, 1160–1166.
16. Pappas, D.K.; Boningari, T.; Boolchand, P.; Smirniotis, P.G. Novel manganese oxide confined interweaved titania nanotubes for the low-temperature selective catalytic reduction (SCR) of NO<sub>x</sub> by NH<sub>3</sub>. *J. Catal.* **2016**, *334*, 1–13.
17. Ettireddy, P.R.; Ettireddy, N.; Boningari, T.; Pardemann, R.; Smirniotis, P.G. Investigation of the selective catalytic reduction of nitric oxide with ammonia over Mn/TiO<sub>2</sub> catalysts through transient isotopic labeling and in situ FT-IR studies. *J. Catal.* **2012**, *292*, 53–63.
18. Smirniotis, P.G.; Peña, D.A.; Uphade, B.S. Low-Temperature Selective Catalytic Reduction (SCR) of NO with NH<sub>3</sub> by Using Mn, Cr, and Cu Oxides Supported on Hombikat TiO<sub>2</sub>. *Angew. Chem. Int. Ed. Eng.* **2001**, *40*, 2479–2482.
19. Singoredjo, L.; Korver, R.; Kapteijn, F.; Moulijn, J. Alumina supported manganese oxides for the low-temperature selective catalytic reduction of nitric oxide with ammonia. *Appl. Catal. B* **1992**, *1*, 297–316.
20. Ma, K.; Zou, W.X.; Zhang, L.; Li, L.L.; Yu, S.H.; Tang, C.J.; Gao, F.; Dong, L. Construction of hybrid multi-shell hollow structured CeO<sub>2</sub>-MnO<sub>x</sub> materials for selective catalytic reduction of NO with NH<sub>3</sub>. *RSC Adv.* **2017**, *7*, 5989–5999.
21. Liu, C.; Gao, G.; Shi, J.W.; He, C.; Li, G.D.; Bai, N.; Niu, C. MnO<sub>x</sub>-CeO<sub>2</sub> shell-in-shell microspheres for NH<sub>3</sub>-SCR de-NO<sub>x</sub> at low temperature. *Catal. Commun.* **2016**, *86*, 36–40.
22. Qi, G.; Yang, R.T.; Chang, R. MnO<sub>x</sub>-CeO<sub>2</sub> mixed oxides prepared by co-precipitation for selective catalytic reduction of NO with NH<sub>3</sub> at low temperatures. *Appl. Catal. B Environ.* **2004**, *51*, 93–106.
23. Hu, H.; Zha, K.; Li, H.; Shi, L.; Zhang, D. In situ DRIFTS investigation of the reaction mechanism over MnO<sub>x</sub>-MO<sub>y</sub>/Ce<sub>0.75</sub>Zr<sub>0.25</sub>O<sub>2</sub> (M = Fe, Co, Ni, Cu) for the selective catalytic reduction of NO<sub>x</sub> with NH<sub>3</sub>. *Appl. Sur. Sci.* **2016**, *387*, 921–928.
24. Xiao, F.; Gu, Y.; Tang, Z.; Han, F.; Shao, J.; Xu, Q.; Zhu, H. ZrO<sub>2</sub> Modified MnO<sub>x</sub>/Attapulgite Catalysts for NH<sub>3</sub>-SCR of NO at Low Temperature. *J. Chem. Eng. Jpn.* **2015**, *48*, 481–487.
25. Xie, A.; Zhou, X.; Huang, X.; Ji, L.; Zhou, W.; Luo, S.; Yao, C. Cerium-loaded MnO<sub>x</sub>/attapulgite catalyst for the low-temperature NH<sub>3</sub>-selective catalytic reduction. *J. Ind. Eng. Chem.* **2017**, *49*, 230–241.

26. Chmielarz, L.; Kuśtrowski, P.; Dziembaj, R.; Cool, P.; Vansant, E.F. Selective catalytic reduction of NO with ammonia over porous clay heterostructures modified with copper and iron species. *Catal. Today* **2007**, *119*, 181–186.
27. Hou, X.X.; Schmiege, S.J.; Wei, L.; Epling, W.S. NH<sub>3</sub> pulsing adsorption and SCR reactions over a Cu-CHA SCR catalyst. *Catal. Today* **2012**, *197*, 9–17.
28. Schmiege, S.J.; Oh, S.H.; Kim, C.H.; Brown, D.B.; Lee, J.H.; Pedenc, C.H.F.; Kim, D.H. Thermal durability of Cu-CHA NH<sub>3</sub>-SCR catalysts for diesel NO<sub>x</sub> reduction. *Catal. Today* **2012**, *184*, 252–261.
29. Brookshear, D.W.; Nam, J.G.; Ke, N.; Toops, T.J.; Binder, A. Impact of sulfation and desulfation on NO<sub>x</sub> reduction using Cu-chabazite SCR catalysts. *Catal. Today* **2015**, *258*, 359–366.
30. Luo, S.; Zhou, W.; Xie, A.; Wu, F.; Yao, C.; Li, X.; Zuo, S.; Liu, T. Effect of MnO<sub>2</sub> polymorphs structure on the selective catalytic reduction of NO<sub>x</sub> with NH<sub>3</sub> over TiO<sub>2</sub>-Palygorskite. *Chem. Eng. J.* **2016**, *286*, 291–299.
31. Chmielarz, L.; Kuśtrowski, P.; Piwowska, Z.; Dudek, B.; Gil, B.; Michalik, M. Montmorillonite, vermiculite and saponite based porous clay heterostructures modified with transition metals as catalysts for the DeNO<sub>x</sub> process. *Appl. Catal. B Environ.* **2009**, *88*, 331–340.
32. Samojeđen, B.; Moždzeń, M. The influence of amount of copper of modified vermiculites on catalytic properties in SCR-NH<sub>3</sub>. *Energy Fuels* **2017**, *14*, 02020.
33. Ying, S. Preparation and Properties of Vermiculite Supported TiO<sub>2</sub> Photocatalyst. *Chin. J. Inorg. Chem.* **2011**, *27*, 40–46.
34. Li, P.; Zhu, M.; Dan, J.; Kang, L.; Lai, L.; Cai, X.; Zhang, J.; Yu, F.; Tian, Z.; Dai, B. Two-dimensional porous SiO<sub>2</sub> nanomesh supported high dispersed Ni nanoparticles for CO methanation. *Chem. Eng. J.* **2017**, *326*, 774–780.
35. Li, P.; Wen, B.; Yu, F.; Zhu, M.; Guo, X.; Han, Y.; Kang, L.; Huang, X.; Dan, J.; Ouyang, F.; et al. High efficient nickel/vermiculite catalyst prepared via microwave irradiation-assisted synthesis for carbon monoxide methanation. *Fuel* **2016**, *171*, 263–269.
36. Huang, X.; Yu, F.; Zhu, M.; Ouyang, F.; Dan, J. Hydrochlorination of acetylene using expanded multilayered vermiculite (EML-VMT)-supported catalysts. *Chin. Chem. Lett.* **2015**, *26*, 1101–1104.
37. Shen, B.; Liu, T.; Zhao, N.; Yang, X.; Deng, L. Iron-doped Mn-Ce/TiO<sub>2</sub> catalyst for low temperature selective catalytic reduction of NO with NH<sub>3</sub>. *J. Environ. Sci. Chin.* **2010**, *22*, 1447–1454.
38. Lin, Q.; Li, J.; Ma, L.; Hao, J. Selective catalytic reduction of NO with NH<sub>3</sub> over Mn-Fe/USY under lean burn conditions. *Catal. Today* **2010**, *151*, 251–256.
39. Thirupathi, B.; Smirniotis, P.G. Co-doping a metal (Cr, Fe, Co, Ni, Cu, Zn, Ce, and Zr) on Mn/TiO<sub>2</sub> catalyst and its effect on the selective reduction of NO with NH<sub>3</sub> at low-temperatures. *Appl. Catal. B Environ.* **2011**, *110*, 195–206.
40. Fan, Z.; Shi, J.W.; Gao, C.; Gao, G.; Wang, B.; Niu, C. Rationally Designed Porous MnO<sub>x</sub>-FeO<sub>x</sub> Nanoneedles for Low-Temperature Selective Catalytic Reduction of NO<sub>x</sub> by NH<sub>3</sub>. *ACS Appl. Mater. Interfaces* **2017**, *9*, 16117.
41. Thirupathi, B.; Smirniotis, P.G. Nickel-doped Mn/TiO<sub>2</sub> as an efficient catalyst for the low-temperature SCR of NO with NH<sub>3</sub>: Catalytic evaluation and characterizations. *J. Catal.* **2012**, *288*, 74–83.
42. Kapteijn, F.; Singoredjo, L.; Andreini, A.; Moulijn, J.A. Activity and selectivity of pure manganese oxides in the selective catalytic reduction of nitric oxides with ammonia. *Appl. Catal. B Environ.* **1994**, *3*, 173–189.
43. Reddy, G.K.; He, J.; Thiel, S.W.; Pinto, N.G.; Smirniotis, P.G. Sulfur-tolerant Mn-Ce-Ti sorbents for elemental mercury removal from flue gas: Mechanistic investigation by XPS. *J. Phys. Chem. C* **2015**, *119*, 8634–8644.
44. Gao, G.; Shi, J.W.; Liu, C.; Gao, C.; Fan, Z.; Niu, C. Mn/CeO<sub>2</sub> catalysts for SCR of NO<sub>x</sub> with NH<sub>3</sub>: Comparative study on the effect of supports on low-temperature catalytic activity. *Appl. Sur. Sci.* **2017**, *411*, 338–346.
45. Li, Y.; Wan, Y.; Li, Y.; Zhan, S.; Guan, Q.; Tian, Y. Low-Temperature Selective Catalytic Reduction of NO with NH<sub>3</sub> over Mn<sub>2</sub>O<sub>3</sub>-doped Fe<sub>2</sub>O<sub>3</sub> Hexagonal Microsheets. *ACS Appl. Mater. Interfaces* **2016**, *8*, 5224–5233.
46. Zhang, J.; Qu, H. Low-temperature selective catalytic reduction of NO<sub>x</sub> with NH<sub>3</sub> over Fe–Cu mixed oxide/ZSM-5 catalysts containing Fe<sub>2</sub>CuO<sub>4</sub> phase. *Res. Chem. Interfaces* **2015**, *41*, 4961–4975.
47. Lin, Z.; Lei, Z.; Qu, H.; Qin, Z. A study on chemisorbed oxygen and reaction process of Fe-CuO<sub>x</sub>/ZSM-5 via ultrasonic impregnation method for low-temperature NH<sub>3</sub>-SCR. *J. Mol. Catal. A Chem.* **2015**, *409*, 207–215.

48. Haidi, X.U.; Fang, Z.; Cao, Y.; Kong, S.; Lin, T.; Gong, M.; Chen, Y. Influence of Mn/(Mn + Ce) Ratio of MnO<sub>x</sub>-CeO<sub>2</sub>/WO<sub>3</sub>-ZrO<sub>2</sub> Monolith Catalyst on Selective Catalytic Reduction of NO<sub>x</sub> with Ammonia. *Chin. J. Catal.* **2012**, *33*, 1927–1937.
49. Fang, C.; Zhang, D.; Cai, S.; Zhang, L.; Huang, L.; Li, H.; Maitarad, P.; Shi, L.; Gao, R.; Zhang, J. Low-temperature selective catalytic reduction of NO with NH<sub>3</sub> over nanoflaky MnO<sub>x</sub> on carbon nanotubes in situ prepared via a chemical bath deposition route. *Nanoscale* **2013**, *5*, 9199–9207.
50. Boningari, T.; Ettireddy, P.R.; Somogyvari, A.; Liu, Y.; Vorontsov, A.; McDonald, C.A.; Smirniotis, P.G. Influence of elevated surface texture hydrated titania on Ce-doped Mn/TiO<sub>2</sub> catalysts for the low-temperature SCR of NO<sub>x</sub> under oxygen-rich conditions. *J. Catal.* **2015**, *325*, 145–155.
51. Khan, A.; Smirniotis, P.G. Relationship between temperature-programmed reduction profile and activity of modified ferrite-based catalysts for WGS reaction. *J. Mol. Catal. A Chem.* **2008**, *280*, 43–51.
52. Cai, S.; Hu, H.; Li, H.; Shi, L.; Zhang, D. Design of multi-shell Fe<sub>2</sub>O<sub>3</sub>@MnO<sub>x</sub>@CNTs for the selective catalytic reduction of NO with NH<sub>3</sub>: Improvement of catalytic activity and SO<sub>2</sub> tolerance. *Nanoscale* **2016**, *8*, 3588–3598.
53. Liu, Z.; Zhu, J.; Li, J.; Ma, L.; Woo, S.I. Novel Mn-Ce-Ti mixed-oxide catalyst for the selective catalytic reduction of NO<sub>x</sub> with NH<sub>3</sub>. *ACS Appl. Mater. Interfaces* **2014**, *6*, 14500–14508.
54. France, L.J.; Yang, Q.; Li, W.; Chen, Z.; Guang, J.; Guo, D.; Wang, L.F.; Li, X.H. Ceria modified FeMnO<sub>x</sub>-Enhanced performance and sulphur resistance for low-temperature SCR of NO<sub>x</sub>. *Appl. Catal. B Environ.* **2017**, *206*, 203–215.
55. Kobayashi, M.; Miyoshi, K. WO<sub>3</sub>-TiO<sub>2</sub> monolithic catalysts for high temperature SCR of NO by NH<sub>3</sub>: Influence of preparation method on structural and physico-chemical properties, activity and durability. *Appl. Catal. B Environ.* **2007**, *72*, 253–261.
56. Qiu, Y.; Liu, B.; Du, J.; Tang, Q.; Liu, Z.; Liu, R.; Tao, C. The monolithic cordierite supported V<sub>2</sub>O<sub>5</sub>-MoO<sub>3</sub>/TiO<sub>2</sub> catalyst for NH<sub>3</sub>-SCR. *Chem. Eng. J.* **2016**, *294*, 264–272.
57. Hwang, J.; Ha, H.J.; Ryu, J.; Choi, J.J.; Ahn, C.W.; Kim, J.W.; Hahn, B.D.; Yoon, W.H.; Lee, H.; Choi, J.H. Enhancement of washcoat adhesion for SCR catalysts to convert nitrogen oxide using powder spray coating of TiO<sub>2</sub> on metallic honeycomb substrate. *Catal. Commun.* **2017**, *94*, 1–4.
58. Gan, L.; Lei, S.; Yu, J.; Ma, H.; Yamamoto, Y.; Suzuki, Y.; Xu, G.; Zhang, Z. Development of highly active coated monolith SCR catalyst with strong abrasion resistance for low-temperature application. *Front. Environ. Sci. Eng.* **2015**, *9*, 979–987.
59. Huang, H.F.; Jin, L.L.; Lu, H.F.; Yu, H.; Chen, Y.J. Monolithic Cr-V/TiO<sub>2</sub>/cordierite catalysts prepared by in-situ precipitation and impregnation for low-temperature NH<sub>3</sub>-SCR reactions. *Catal. Commun.* **2013**, *34*, 1–4.
60. Gao, C.; Shi, J.W.; Fan, Z.; Niu, C. Sulfur and Water Resistance of Mn-Based Catalysts for Low-Temperature Selective Catalytic Reduction of NO<sub>x</sub>: A Review. *Catalysts* **2018**, *8*, 11.

